SURFACE FAULTING AND GROUND DEFORMATION: CONSIDERATIONS ON THEIR LOWER DETECTABLE LIMIT AND ON FDHA FOR NUCLEAR INSTALLATIONS.

L. Serva[a)], F.A. Livio[b)] , A. Gürpinar[c)]

Abstract

We performed a review of a representative dataset on coseismic surface deformation, derived from both InSAR imaging and from traditional field survey of surface faulting. This analysis indicates a minimum threshold value of Mw 5.4 - 5.5 for earthquake-induced ground deformation and faulting, with an inherently lower limit of detection that makes hard to recognize surface deformation caused by Mw < 4.5 – 5.0 events. Significant exceptions are represented by shallow (i.e., less than ca. 5 km) events that occur in volcano-tectonic settings, where surface deformation and dislocation are clearly detectable also for Mw ca. 4.0.
Furthermore, a statistically significant regression between the areal extent of surface deformation and maximum slip at surface is proposed. This correlation is discussed in relation to the Fault Displacement Hazard Analysis (FDHA) for nuclear power plants. In particular, the deformation area is used in order to find a potential solution for the second and the third criterion for defining a capable fault, *sensu* IAEA SSG-9, 2010.

1. INTRODUCTION

Recently, remote sensing (i.e., RADAR interferometry – InSAR, differential LiDAR, optical imagery correlation) greatly improved the detecting possibilities for surface faulting and ground deformation and changed the analytical approach to earthquake-induced ground deformation. InSAR imaging allows to measure the regional permanent ground deformation induced by earthquakes, down to a cm-scale resolution, over areas of hundreds of square kilometers. The observed coseismic deformation fields can be inverted to derive the parameters of the seismogenic source, similarly to what is usually done with geodetic and strong motion data. Such an approach is informative for moderate and larger earthquakes and, since the late 1990's, it expanded earthquake geology knowledge.

So far, systematic databases of earthquake-induced ground ruptures result in well-accepted scaling relations between earthquake size (i.e., usually expressed as moment magnitude Mw) and dimensions of the seismogenic structure (i.e., area, length, max. displacement). Accordingly, recent works (e.g., Livio et al., 2017; Gürpinar et al., 2017) pointed out a similar close relationship between the areal extent and amount of surface deformation, as measured through InSAR imaging, and earthquake size.

Still, a new issue arises on the lower limit of detection for surface faulting and ground deformation, based on both traditional survey and InSAR-derived displacement fields. These two sources of information need to be integrated into comprehensive databases, as underlined by scientific working groups on this issue (e.g., surface rupture database – SURE, http://www.earthquakegeology.com/index.php?page=surface&s=4). The published databases of observations of surface faulting are relatively poor in the region of low Mw earthquakes, and some doubts are arising on their completeness and on possible epistemic uncertainties deriving from biased datasets (e.g., Stirling et al. 2002).

In this paper we: i) review the lower Mw limit for surface faulting according to published databases; ii) inspect the lower limit of detection for ground deformation from InSAR imaging; iii) discuss the relationship between the ground deformation and the potential for surface faulting (fault capability) in relation to FDHA and, in particular, as it relates to nuclear power plant safety.

2. AN ANALYSIS OF THE SURFACE FAULTING VS MW REGRESSION CURVES AND A POTENTIAL INFERENCE ON THE LOWER LIMIT OF MW FOR SURFACE FAULTING

In the present practice of fault displacement hazard analysis (FDHA; ANSI/ANS-2.30, 2015), the possibility that an earthquake of given magnitude will result in surface faulting is considered using empirical relationships which are mainly based on field observations of past ground ruptures.

Statistical analysis is performed as a regression of conditional probability of occurrence (P) on datasets of past historical and instrumental events. Results from some of the most accepted works in literature are reported in **Errore. L'origine riferimento non è stata trovata.**, showing that for normal and strike-slip faulting events, P increases above Mw ≥ 5.5 and results in a ca. 95% probability of occurrence for earthquakes Mw 7.0. The studies here reported considered a dataset of 100 events between Mw 4.5 and 7.6, mainly representing the Mw 5.5 to 7.0 interval. It is important, therefore, to recall that the calculated probabilities are sample-dependent and prone to change when sample size and characteristics are altered.

Such studies show a correlation in the proposed regressions, generally assuming a log-linear relationship between Mw and rupture characteristics (i.e., length, area, displacement etc.). It is implicit in the logarithmic nature of the calculated regressions, that progressively lower values of rupture length and displacements are expected for decreasing Mw, resulting in considerably small values, when extrapolated for low Mw ranges (i.e., Mw ≤ 4.5).

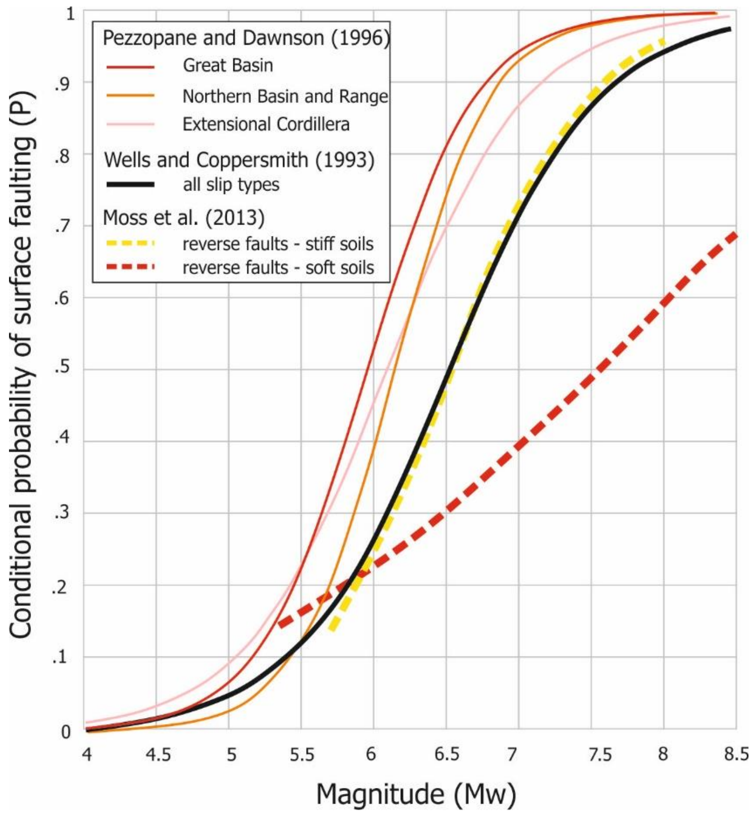

Figure 1. Conditional probability curves for primary surface faulting in relation to different earthquakes magnitudes and kinematics.

Below, we summarize our analysis on the state of the art of these regressions and highlight some of the shortcomings, as recognized by previous analytical works.

Data completeness. Wells and Coppersmith (1994) published empirical relationships, considering a dataset of the 244 worldwide earthquakes available at the time. The authors provide a range of Mw for the applicability of each calculated regression and consider both the entire dataset or subsets of events according to earthquake kinematics but the dataset was analyzed with insufficient consideration on the data accuracy (i.e., instrumental vs pre-instrumental earthquakes) and with the restriction Mw ≥ 4.5 (Stirling et al., 2002). Other regressions have been later published and a complete summary of these is provided by Stirling et al. (2013) who reviewed 72 models that are available in literature, grouping them by different tectonic regimes and style of faulting and ranking them according to performance and reliability.

Data completeness is questioned by the Mw range of the considered earthquakes. In fact, the Mw lower bound of these datasets (i.e., median Mw 5.6; Figure 2a) is close to the Mw value at which the conditional probability of surface faulting occurrence starts to increases (cfr. Figure 1).

Data reliability. It is noteworthy to recall that Stirling et al. (2002) observed that estimates of surface rupture displacement and magnitude for crustal earthquakes from the pre-instrumental era (pre-1900) tend to be greater than the corresponding estimates derived from modern scaling relations (Figure 2b). They used an expanded and updated version of the earthquake dataset of Wells and Coppersmith (1994) including pre-instrumental (orange dots and line in Figure 2b) and instrumental data (blue dots and line in Figure 2b) and data originally excluded from the Wells and Coppersmith (1994) dataset. Updated regressions reduce but do not remove the differences. Instead, the remaining differences appear to be due to natural censoring of the traces of earthquakes with short surface rupture lengths and small displacements from the pre-instrumental record, due to scarp degradation processes.

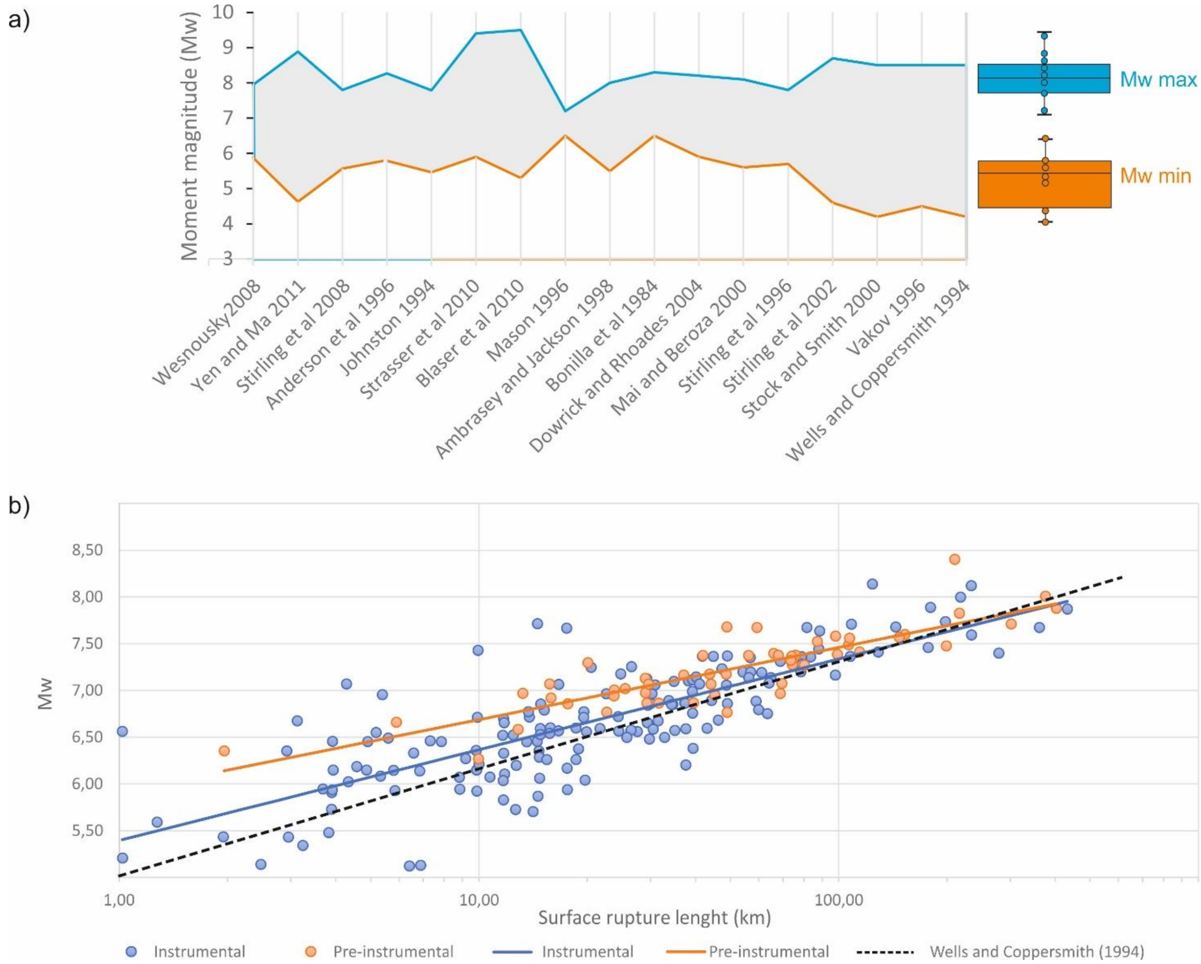

Figure 2. (a) Range of Mw used in the datasets of several published empirical regressions (for a comprehensive analysis see Stirling, 2013, from where the data were derived), boxplots summarize the value distribution for upper and lower limit of datasets; (b) regressions of magnitude versus surface rupture length (modified after Stirling et al., 2002); regression from Wells and Coppersmith (1994) is also reported, note the substantially diverging predictions for the lower values of Mw, close to the lower limit of the dataset.

Earthquake dynamics and kinematics. When determining maximum magnitude on faults using these regression equations, the earthquake dynamics and kinematics are generally neglected, with some notable exceptions. Anderson et al. (1996) included the fault slip rate as a variable in empirical regressions, obtaining more accurate predictions. Mohammadioun and Serva (2001) proposed a theoretical relationship between earthquake size (Ms) and rupture length, including stress drop as an additional parameter (**Errore. L'origine riferimento non è stata trovata.**). The rupture length expected for any given Ms, will depend on the assumed stress drop, a value closely related to the seismotectonic environment.

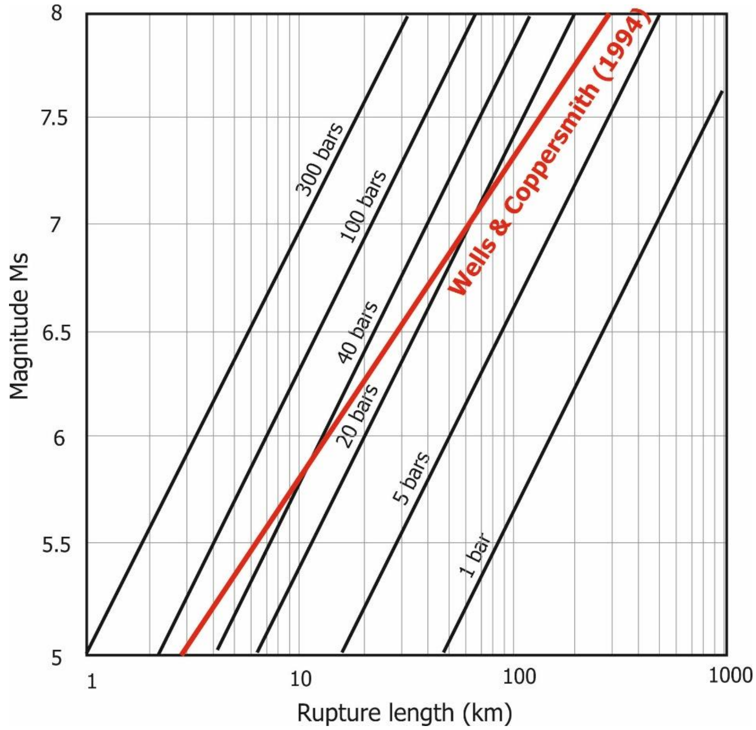

Figure 3. Scaling law for various levels of stress drop (in bars), showing the relationship between surface-wave magnitude (Ms) and rupture length (black solid lines); the empirical relationship after Wells and Coppersmith (1994) is shown (red solid line) as a reference (redrawn after Mohammadioun and Serva, 2001).

Seismotectonic setting. Stirling et al. (2013) review discuss the indiscriminate aggregation of seismogenic sources taken from very diverse geological settings, by using these regressions with little consideration of the regional seismotectonic environment. Mohammadioun and Serva (2001) discussed such inconsistencies, considering an earthquake database of shallow volcano-tectonic events collected in the Etna volcano area (data after Azzaro et al., 2000, Figure 4).

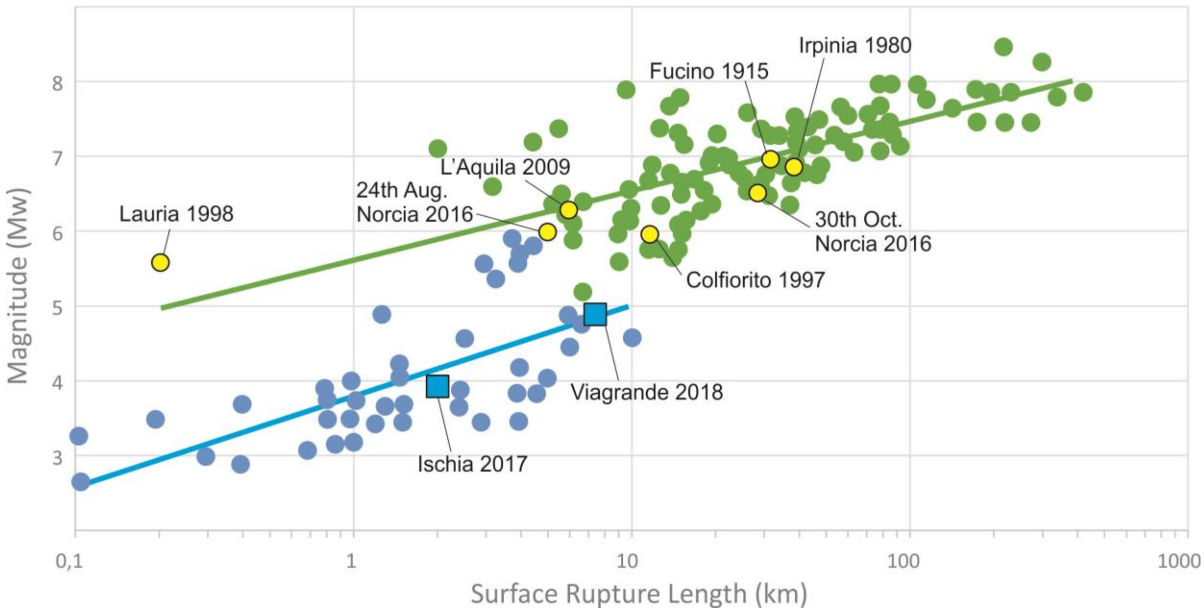

Figure 4. Empirical regression of surface rupture length vs Mw for a dataset of volcano-tectonic earthquakes in the Mt.Etna area (blue dots and line for best fit; data after Azzaro et al., 2000) compared with data from Wells and Coppersmith (1994) (green dots and line) and Apennines earthquakes (yellow dots; data after Michetti et al. 1996; Vittori et al., 2000; Blumetti et al., 2002; Vittori et al., 2011; Livio et al., 2016; Civico et al., 2018). We included also two recent and well-documented volcano-tectonic Italian earthquakes (blue squares): the Aug. 21, 2017, Ischia earthquake - Mw 3.9 , focal depth 1.2 km (Nappi et al., 2018), and the Dec. 26, 2018 Viagrande earthquake - Mw 4.9, focal depth < 1 km (EMERGEO Working Group, 2019). Note the good fitting of these two events with the database reported in Mohammadioun and Serva (2001).

So far, we can conclude that, for crustal earthquakes not related to a volcano-tectonic environment, published statistical models indicate a Mw close to 5.5 as the lower limit for surface faulting with an associated rupture length, derived from empirical regressions, on the order of a few kilometers. The extrapolation of calculated regressions in the region of smaller Mw is not currently supported by an adequate dataset. One of the main sources of uncertainty in the present datasets comes from the heterogeneity of the tectonic settings and from the objective limits posed by traditional geologic mapping accuracy and/or biased sampling during field data collection. Similarly, it is a fact that no surface faulting has been documented, until present, for crustal earthquakes below Mw 5.0. This is because either the data based on field observations are insufficient or because smaller magnitudes do not produce surface faulting. In order to investigate the two possibilities, in the next chapter we will discuss the data coming from InSAR imaging on the earthquake-induced surface deformation.

3. LOWER LIMIT OF MW FOR EARTHQUAKE-INDUCED GROUND DEFORMATION: INSIGHTS FORM INSAR IMAGING.

The above discussion indicates an apparent lower limit of Mw for earthquake-induced ground deformation, based on the analysis of empirical datasets of surface faulting. A similar approach has been recently used for the regression of the areal extent of earthquake-induced ground deformation against Mw (e.g., Livio et al., 2017; Gurpinar et al., 2017). We here update that regression, including some recent earthquakes and adopting the same methods, as summarized below.

In a GIS environment, we measured the areal extent (square kilometers) of coseismic ground deformation for selected earthquakes of different Mw. We mapped the area enclosed by certain fringes (i.e., coherent and continuous signal) from InSAR imaging (Figure 5).

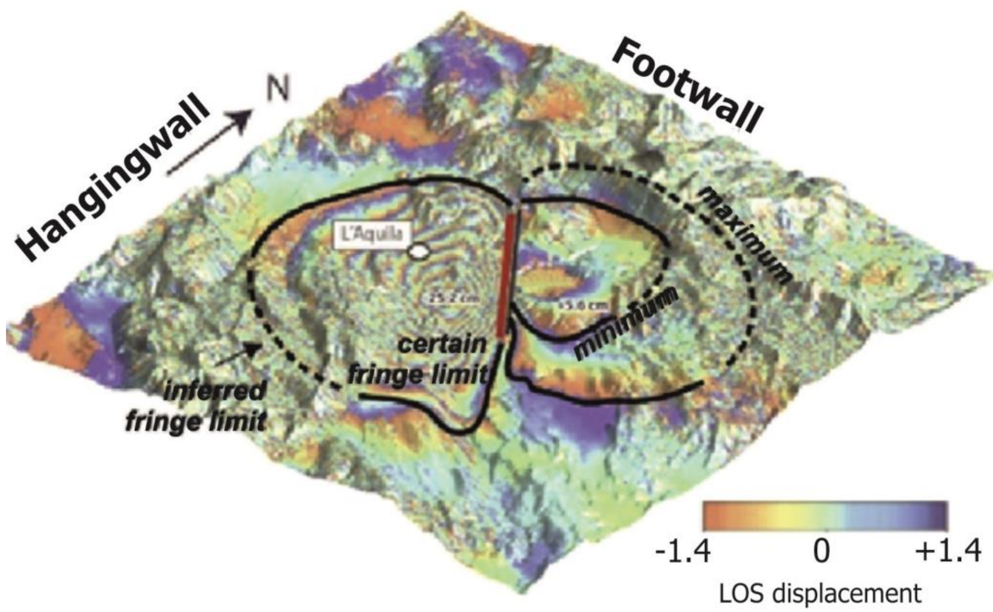

Figure 5. Assumed method for area calculation: typical observed versus inferred fringe limits and uncertainties in the locations of the most external coherent fringes are indicated (modified after Livio et al., 2017).

In Table 1 we listed the earthquakes used for this correlation and the measured values. We selected the most significant earthquakes worldwide imaged through InSAR in order to represent different kinematics, depths (km 2 – 30) and magnitude intervals (Mw 4.2 – 9.0). Part of these (31 events) have already been presented in a previous paper (Livio et al., 2017).

First, we verified the published regression using, as a validation dataset, 18 more earthquakes which occurred in the period 2016-2018. It is noteworthy that almost all the earthquakes of this validation dataset lie within the 95% confidence interval of the proposed regression (Figure 6).

Table 1. Earthquakes used for regression analysis. Legend: Mw, moment magnitude; Kin., prevailing earthquake kinematics (N, normal faulting; TH, thrust faulting; S, strike-slip faulting); Ref., reference for earthquake InSAR imaging.

Dataset after Livio et al. (2017)

Date (dd/mm/yyyy)	Earthquake	Mw	Depth (km)	Kin.	Area (sq. km)	Ref.
28/06/1992	Landers	7.30	1.09	S	6130	Massonnet et al. (1993)
17/05/1993	Eureka Valley	6.10	13	N	640	Peltzer & Rosen (1995)
24/02/1994	Sefidabeh	6.20	9	TH	1706	Parsons et al. (2006)
08/11/1997	Mainji	7.60	22	S	13866	Funning et al. (1997)
30/04/1999	Zagros	5.30	4	TH	109.8	Lohman & Simons, (2005)
17/08/1999	Izmit	7.40	17	S	11230	Delouis et al. (2002)
07/09/1999	Athens	5.90	10	N	233	Baumont et al. (2004)
16/10/1999	Hector Mine	7.10	14	S	6715	Simons et al. (2002)
12/11/1999	Duzce	7.20	14	S	3888	Burgmann et al. (2002)
22/12/1999	Ain Temouchent	5.70	5	TH	230	Belabbes et al. (2009)
06/06/2000	Orta– Çankırı	6.00	8	N	321	Taymaz et al. (2007)
26/12/2003	Bam	6.60	10	S	554	Fialko et al. (2005)
24/02/2004	Al Hoceima	6.50	13	S	222	Cakir et al. (2006)
20/07/2005	Hatanbulag	5.20	6	TH	120.53	Amarjargal et al. (2013)
21/09/2005	Kalannie	4.40	1	S	7.14	Dawson et al. (2008)
08/10/2005	Kashmir	7.60	10	TH	3021	Pathier et al. (2006)
10/10/2007	Katanning	4.70	1	S	5.61	Dawson et al. (2008)
19/01/2008	Busiin Gol	5.10	8	N	179	Amarjargal et al. (2012)
25/04/2008	Reno-Mogul	4.70	2	S	150	Bell et al. (2012)
06/04/2009	L'Aquila	6.30	8.8	N	652	Walters et al. (2009)
19/05/2009	Harrat Lunayyr	5.70	8	N	341	Pallister et al. (2010)
12/01/2010	Haiti	7.00	13	S	1616	Lepinay et al. (2011)
22/02/2011	Christchurch	6.42	5	S	2269	Elliott et al. (2012)

11/03/2011	Tohoku	9.00	30	TH	185581	Kobayashi et al. (2011)
23/10/2011	Van	7.10	7.2	TH	1310	Dogan & Karakas (2013)
20/05/2012	Emilia 1	5.86	5	TH	350	Bignami et al. (2012)
29/05/2012	Emilia 2	5.66	9.6	TH	325	Bignami et al. (2012)
24/08/2014	Napa Valley	6.00	10	S	348	http://aria.jpl.nasa.gov/node/39
25/04/2015	Nepal	7.8	15	TH	28831	http://www.gsi.go.jp/cais/topic150429-index.html
07/12/2015	Tajikistan	7.20	26	TH	3580	http://www.gsi.go.jp/cais/topic160115-index-e.html
New dataset (this study)						
Date (dd/mm/yyyy)	Earthquake	Mw	Depth (km)	Kinematics (*)	Area (sq. km)	Ref.
18/09/2004	Mono lake	5.60	3	S	209	Lee et al. (2017)
16/04/2016	Kunamoto	7.00	10	S	813	http://www.gsi.go.jp/cais/topic160428-index-e.html
24/08/2016	Amatrice	6.20	4	N	270	http://www.gsi.go.jp/cais/topic160826-index-e.html
21/10/2016	Tottori	6.60	10	S	513	http://www.gsi.go.jp/cais/topic161027-index-e.html
26/10/2016	Visso	5.90	8	N	367	Cheloni et al. (2017)
30/10/2016	Norcia	6.60	9	N	719	http://www.gsi.go.jp/cais/topic161108-index-e.html
13/11/2016	Kaikoura - New Zealand	7.80	15	S	18682	http://www.gsi.go.jp/cais/topic161027-index-e.html
12/01/2017	Iran	6.00	9	TH	175	http://sarviews-hazards.alaska.edu/Event/41/
21/08/2017	Ischia	3.90	3	N	7	http://www.irea.cnr.it/en/index.php?option=com_k2&view=item&id=589
12/11/2017	Iraq	7.30	19	TH	5184	http://www.gsi.go.jp/cais/topic171115-index-e.html
17/11/2017	Nyingchi - China	6.40	8	TH	1772	http://sarviews-hazards.alaska.edu/Event/40/
12/12/2017	Kerman - Iran	6.00	10	TH	141	http://sarviews-hazards.alaska.edu/Event/45/
06/02/2018	Taiwan	6.40	17	S	100	http://www.gsi.go.jp/cais/topic180209-index-e.html
16/02/2018	Oaxaca - Mexico	7.20	22	TH	1124	https://disasters.nasa.gov/oaxaca-mexico-earthquake-2018
16/02/2018	Pinotepa de Don Luis - Mexico	7.20	43	TH	4321	http://sarviews-hazards.alaska.edu/Event/61/

25/02/2018	Papua New Guinea	7.50	25	TH	5761	http://www.gsi.go.jp/cais/topic180301-index-e.html
01/11/2018	Pyu - Burma	6.00	10	TH	282	http://sarviews-hazards.alaska.edu/Event/52/

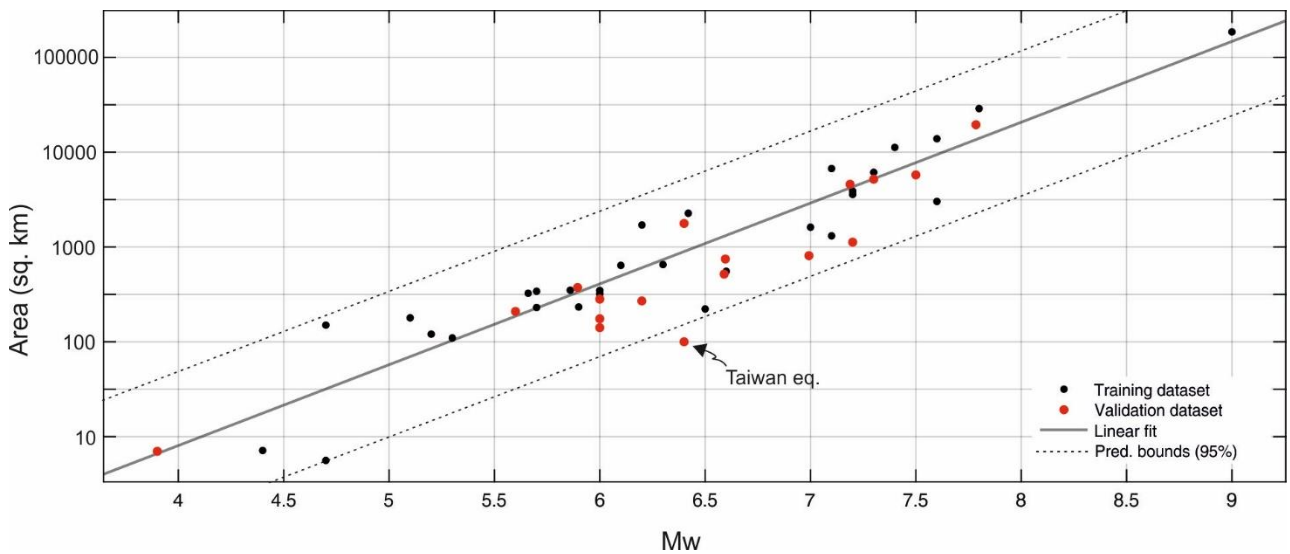

Figure 6. Comparison of the regression of deformed area vs Mw, as proposed in Livio et al. (2017), tested over a dataset (n. = 10) of earthquakes occurred: almost all the earthquakes lies in the 95% bounds of the proposed regression.

Then, we considered the entire and updated dataset and performed a bivariate regression analysis including also other variables. Depth is positively but not strongly correlated with the deformed area (i.e., adjusted R-square 0.3795) and with Mw (i.e., adjusted R-square 0.4447), as expected if we consider that dimensions of seismogenic structures rupturing the upper crust scale with Mw. So, consistently with Livio et al. (2017), depth can be ignored in further analysis. Furthermore, earthquake kinematics is not strongly influencing our regression and a similar data distribution is common for normal, reverse or strike slip modes. So, the stronger dependency of the deformed area is observed on earthquake Mw.

A simple log-linear regression of the deformed areas with Mw has been tested in the following form:

$$Log_{10} A = a(Mw) + b \quad (1)$$

where A is the deformed area (in square km), Mw is the moment magnitude, a and b are parameters (Figure 7). Best fit parameters and intervals for 95% confidence bounds are reported in Table 2 and regression scores in Table 3.

Table 2. Best fit parameters for linear regression analysis.

Parameter	Best fit	95% confidence interval
a	0.8401	0.7378, 0.9424
b	-2.506	-3.167, -1.844

Table 3. Scores of the best fit linear regression.

Goodness of fit:	
SSE (Log A)	5.352
R-square	0.8587
Adjusted R-square	0.8556
RMSE (Log A):	0.3449

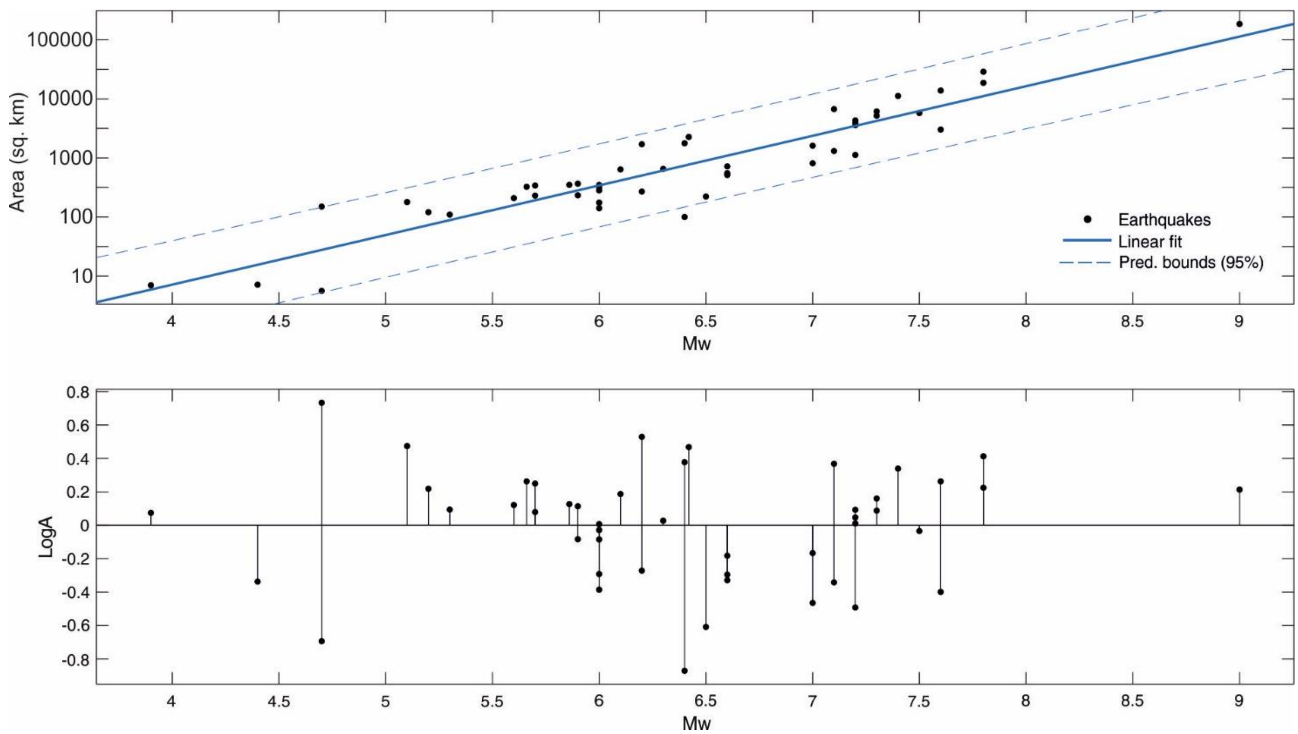

Figure 7. a) Calculated linear regression between deformed area and earthquake magnitude (Mw) and b) residuals plot.

In order to test the expected deformation at surface, we explored different scenarios based on a pure thrust seismogenic structure (Figure 8), according to elastic dislocation models (i.e. Okada, 1985). For modeling, we adopted a uniform slip model on the fault (dip = 30º) and considered the following general parameters: $3.2 * 10^5$ bar for the Young's modulus, 0.25 for the Poisson's ratio, 0.6 for the coefficient of friction. We explored a magnitude (Mw) range between 6.0 and 4.5 and changed the top of the rupture between 0 and 10 km below surface.

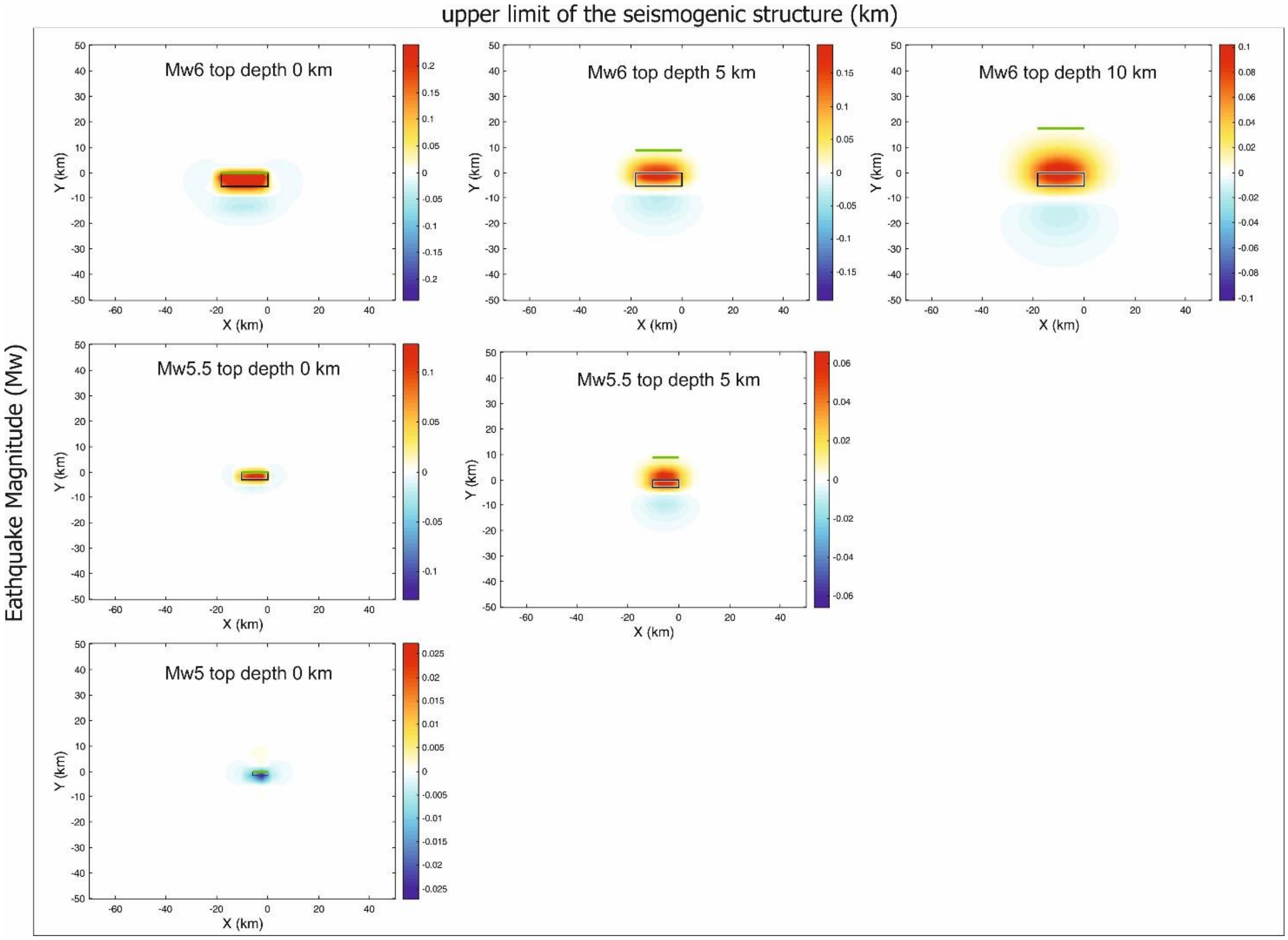

Figure 8. Examples of calculated vertical displacement fields, at surface, at variable earthquake magnitude (Mw) and depth of the top of the seismogenic source for a thrust earthquake: seismogenic source dimensions and slip are determined from earthquake Mw, according to scalar relationships (Wells and Coppersmith, 1994); values of vertical uplift in meters.

We scaled the dimensions and slip on the seismogenic structure according to empirical regressions from Wells and Coppersmith (1994) using equations for thrust faults. Calculations were then performed in Coulomb 3.3 (Toda et al., 2011) obtaining the dislocation components (i.e., Dx, Dy and Dz) of crustal displacement. Since the limit of detection of the InSAR observations is strongly dependent on the observation geometry (LOS distance), we conservatively considered that the observer would be able to measure the real maximum displacement at surface. So, for every considered scenario we calculated the maximum displacement at surface. Results are shown in Figure 9. Our results, are consistent with those discussed in Dawson and Tregoning (2007) on the lower limit of detection through InSAR imaging, and show that below Mw 5.5 only shallow earthquakes (i.e., focal depth < ca. 5 km) can accurately be detected (i.e., with a phase difference ≥ ca. ½ to 1 the sensor wavelength). In fact, the recent Ischia (Mw 3.9) and Valgrande volcano-tectonic earthquakes (Mw 4.9) have been fully imaged through InSAR, thanks to their shallow hypocentral depth (ca. 1.2 km and < 1 km respectively).

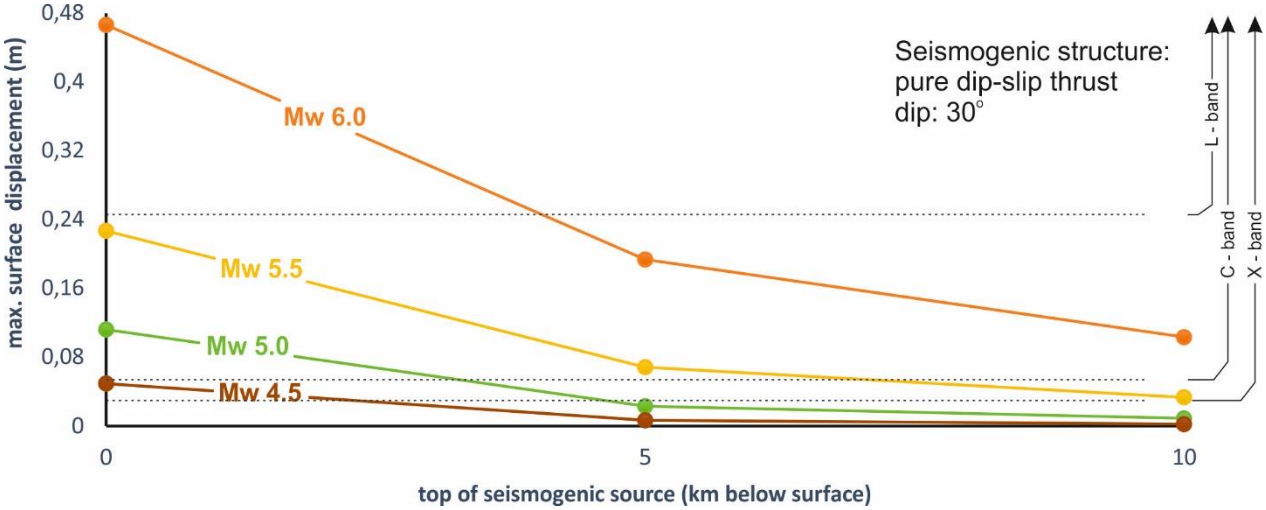

Figure 9. Maximum expected surface displacement according to elastic dislocation models (i.e., Okada, 1985) for a pure dip thrust structure (see the text for details of the modeling parameters); horizontal dashed lines indicate 1 wavelength of different SAR bands, as a possible indicator of lower limit of detection.

Conversely, the direct detection of surface faulting or localized deformation through InSAR imaging is inherently limited by the sensor characteristics and deformation gradients greater than 10^{-5} (X-band) – 10^{-3} (C or L band) result in loss of coherence. Consequently, the direct imaging of surface rupture or near surface blind localized deformation usually results in a linear interruption of the interferogram fringes.

From the discussion above, it emerges that the lack of data below Mw ca. 4.5 is due to an inherent limit of the detection technique. However, as for surface faulting, the expected value of surface deformation is so small that it is unlikely that surface faulting can be detected below this value for crustal earthquakes, not related to volcano-tectonic environment.

The same observation arises from the comparison between the areal extent of earthquake-induced deformation at surface, as derived from InSAR datasets, and maximum slip at surface. We selected 8 recent moderate-to-strong earthquakes and tested a regression between the two variables (Table 4 and Figure 10).

Table 4. Earthquake parameters for some surface faulting events, used for comparison between maximum slip at surface and the area of InSAR-derived surf ace deformation (Figure 10).

Date (dd/mm/yyyy)	Earthquake	Mw	Depth (km)	Kinematics (*)	Area (sq. km)	Log A	Max slip at surface (m)	Ref.
28/06/1992	Landers	7.30	1.09	SR	6130	3.79	7.00	Rymer (1992)

17/08/1999	Izmit	7.40	17	SR	11230	4.05	5.00	Gulen et al. (2002)
16/10/1999	Hector Mine	7.10	14	SR	6715	3.83	5.40	Treiman et al. (2002)
06/04/2009	L'Aquila	6.30	8.8	N	652	2.81	0.15	Vittori et al. (2011)
24/08/2014	Napa Valley	6.00	10	SR	348	2.54	0.46	Brocher et al. (2015)
16/04/2016	Kunamoto	7.00	10	SS	813	2.91	2.20	Shirahama et al. (2016)
24/08/2016	Amatrice	6.00	4	N	270	2.43	0.16	Pucci et al. (2017)
30/10/2016	Norcia	6.50	9	N	719	2.86	2.10	Ferrario et al. (2018)

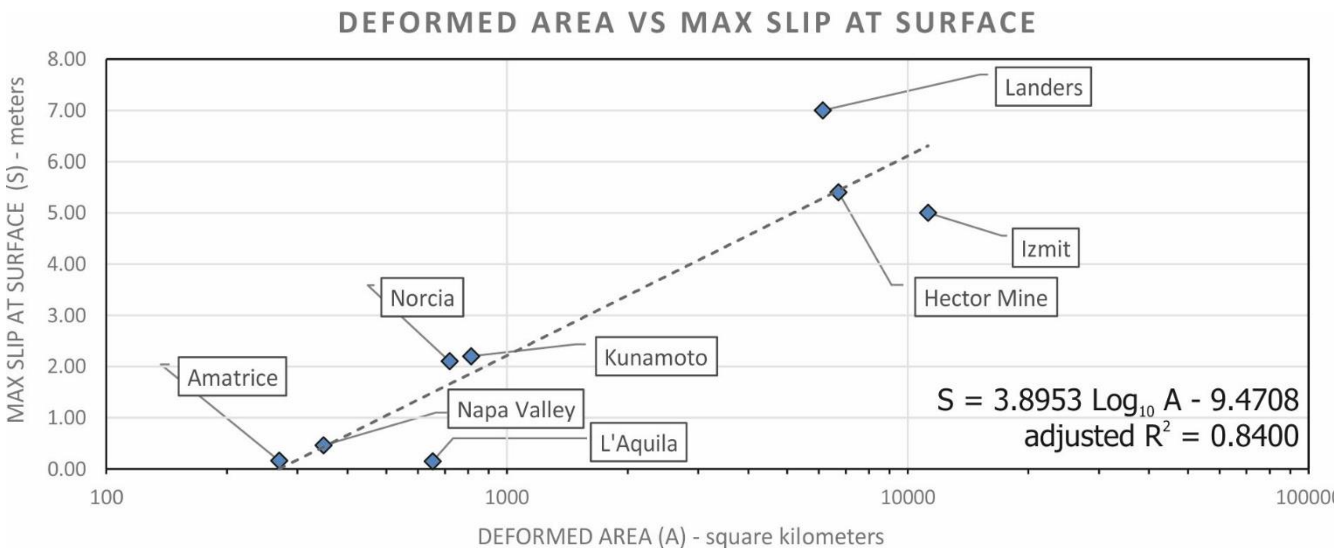

Figure 10. Relationship between maximum slip at surface and InSAR-derived coseismically deformed area; see Table 4 for the sources used as references for surface faulting.

The two variables show a strong positive correlation and suggest that expected maximum slip at surface becomes negligible (i.e., close to zero) for deformed areas under ca. 250 square kilometers (Figure 10), that is a Mw 5.4 – 5.5, according to the previously discussed relationship.

The close spatial relationship between crustal deformation and surface faulting is also underlined in Figure 10, where the traces of the ground ruptures mapped after the Oct. 30th, 2016 Norcia earthquake (Mw 6.5) are mapped on the InSAR-derived coseismic ground deformation. All the mapped fault strands are enclosed in the area interested by coseismic permanent ground deformation, suggesting that crustal strain and static stress transfer played a predominant role, in respect to dynamic triggering, in promoting distributed faulting. This observation, if taken as an assumption, opens the possibility to use the output of simple elastic dislocation models as an input parameter for the assessment of fault capability (*sensu* IAEA, 2010), as will be discussed below.

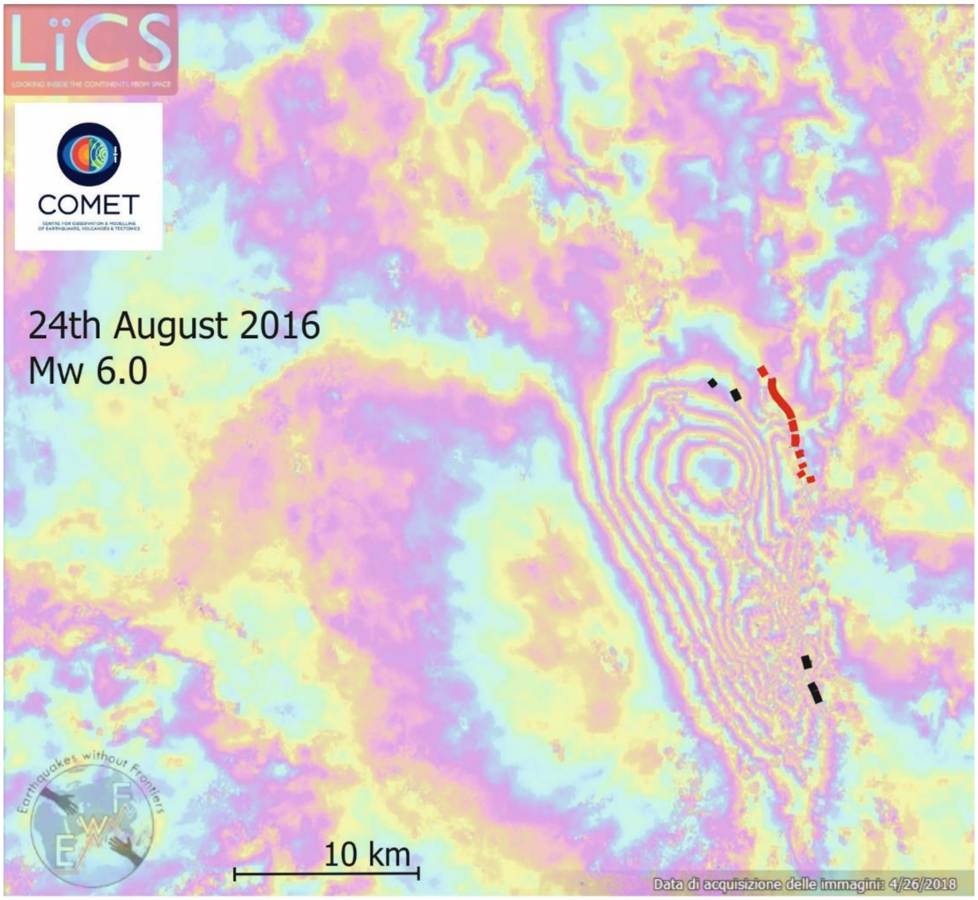
LiCS
COMET
24th August 2016
Mw 6.0
10 km
Data di acquisizione delle immagini: 4/26/2018

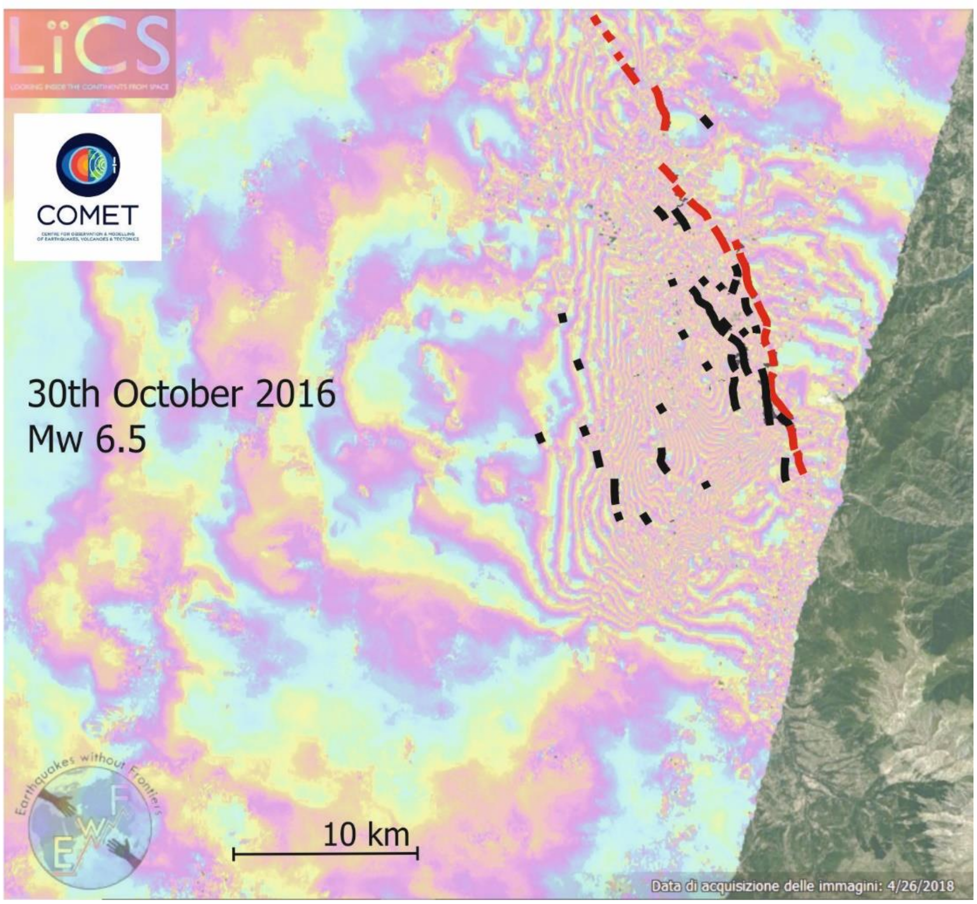
LiCS
COMET
30th October 2016
Mw 6.5
10 km
Data di acquisizione delle immagini: 4/26/2018

Figure 11. Comparison between the extent of InSAR-derived coseismic ground deformation and traces of primary (red) and distributed (black) surface faulting for two mainshocks of the 2016 Central Italy seismic sequence. Fault traces after Livio et al. (2016) and Civico et al. (2018) and InSAR images after Foumelis (2016) and Brcic (2016) for the Aug. 26th and Oct. 30th event respectively.

4. IMPLICATIONS FOR THE FAULT CAPABILITY ASSESSMENT

The strong correlation between the surface faulting and the earthquake-induced crustal deformation at the surface, as discussed previously, can impact on the assessment of the potential for surface faulting and, in particular, on fault capability, sensu IAEA, 2010: a crucial aspect of the seismic hazard evaluation and feasibility of nuclear power plants.

In particular, as stated in the IAEA SSG-9 (2010):

"On the basis of geological, geophysical, geodetic or seismological data, a fault should be considered capable if the following conditions apply:

(a) If it shows evidence of past movement or movements (such as significant deformations and/or dislocations) of a recurring nature within such a period that it is reasonable to conclude that further movements at or near the surface may occur. In highly active areas, where both earthquake data and geological data consistently reveal short earthquake recurrence intervals, periods of the order of tens of thousands of years (e.g. Upper Pleistocene–Holocene, i.e. the present) may be appropriate for the assessment of capable faults. In less active areas, it is likely that much longer periods (e.g. Pliocene–Quaternary, i.e. the present) are appropriate.

(b) If a structural relationship with a known capable fault has been demonstrated such that movement of the one fault may cause movement of the other at or near the surface.

(c) If the maximum potential magnitude associated with a seismogenic structure […], is sufficiently large and at such a depth that it is reasonable to conclude that, in the current tectonic setting of the plant, movement at or near the surface may occur."

While point a) of the quoted text is the main criterion for fault capability and extensively discussed between the involved experts, the conditions expressed in (b) and (c), in our view, are less well understood. These conditions are affected by the correlation between the deformation of the crust and the probability and characteristics of surface faulting.

In fact, when capability, as defined in point a), cannot be assessed because reliable dating is not possible by any available method, including the more updated geochronological dating methods, the fault is considered capable if:

(1) it could be linked with a known capable fault. (i.e. has been demonstrated that a movement of the capable fault may cause movement of such a fault);

(2) - the maximum potential magnitude associated with a seismogenic structure, is sufficiently large and at such a depth that it is reasonable to conclude that, because of the significant crustal deformation produced by the event also in the site vicinity area of the NPP, surface faulting can occur also on faults here located.

Point (1) indicates the capability of an undated fault if it has a structural relationship with a known capable fault. In many cases, this structural relationship may be questionable, therefore an important step forward for a reliable assessment could be the following.

A quantitative approach can rely on the modeling of Coulomb stress transfer between faults (e.g., Stein, 1999): a valuable tool to assess the likelihood of reactivation of preexisting faults, given a primary fault movement. Nevertheless, to accurately model fault reactivation, one must have an *a priori* knowledge of the geometries of the receiving faults, as well as the primary fault itself. In many cases, such detailed information is lacking, and usually only primary fault geometry is well known. Therefore, to predict the probability of a fault to be triggered by another one, a model based solely on primary fault geometry and slip would be needed. We here consider the possibility that triggered faulting could preferentially occur in those sectors where greater strain is induced by co-seismic deformation, that is in those sectors permanently deformed by coseismic ground deformation.

First, it is necessary to identify the deformed area due to the maximum earthquake that may be produced by the capable fault considered, using regressions in Figure 6. In case the deformed area includes the fault under investigation, its potential capability becomes more significant. On the other hand, it becomes less significant in the case the fault is outside the deformed area.

Point (2) indicates a situation where the maximum potential earthquake associated with a seismogenic structure, not necessarily close to the fault under investigation for capability, could produce deformation affecting also the area where this fault is located. To verify this situation, it is proposed to calculate the deformed area using the correlation given in Figure 1 and, if it includes the fault under investigation, it would be necessary to consider this possibility which may lead to an *ad hoc* FDHA.

In point (2) the case of an earthquake of such Mw that surface faulting is expected but there are no geological and geophysical data that could indicate to which structure this earthquake can be associated. In other words, the only source of information would be from the seismological catalogue. In this case, the earthquake should be located near the epicenter given by the seismological database or in its vicinity where potential geological structures exist. Then, the potential deformed area can be calculated, and the process as described above may be followed.

Uncertainties in the various steps provided above should be considered and special emphasis should be given also to the position of the fault under investigation inside the deformed area. In any case, the size of the deformed area would need to be considered with its associated uncertainties calculated by the empirical analysis as outlined above. In treating these uncertainties, the more pessimistic interpretations would need to be considered for fault capability evaluation to comply with the conservative approach used in nuclear industry practices.

5. CONCLUSIONS

In this work, we updated some previously published regressions between coseismically deformed area and earthquake magnitude (Mw), with some recent events. We tested our observations and regressions in the low magnitude range, observing that both crustal deformation and surface faulting show a consistent lower value threshold for detectable surface effects (i.e., Mw 5.4 – 5.5). Interferometric techniques show similar results, with an inherently lower limit of detection that makes hard to recognize surface deformation caused by Mw < 4.5 - 5.0 events. Significant exceptions are represented by events that occur in volcano-tectonic settings, where surface deformation and dislocation is clearly detectable also for Mw as low as ca. Mw 4.0. Furthermore, a correlation between the extent of surface deformation maximum slip at surface is highlighted suggesting surface faulting is close to zero for those earthquakes causing less than ca. 250 square kilometers of surface deformation extent.

We then discuss a potential use of the strong correlation between the surface faulting and the deformation of the crust at the surface in term of the fault displacement hazard assessment (FDHA) for Nuclear Power Plants.

On the basis of the above results coming from the present surface faulting database and the amount of crustal deformation, it will be easier to confirm that, for crustal earthquakes, the lower limit for surface faulting would be approximately Mw 5.5.

While the IAEA Safety Guide SSG-9 provides recommendations related to fault displacement hazards for nuclear installations, the actual application of these recommendations to concrete cases (in particular b) and c) conditions) needs a more quantitative framework. The previous papers by the authors (Livio et al., 2017 and Gürpinar et al., 2017) and the present work constitute an attempt in this direction.

REFERENCES

Amarjargal, S., Kato, T. and Furuya, M., 2013. Surface deformations from moderate-sized earthquakes in Mongolia observed by InSAR, *Earth, Planets and Space* **65**(7), 713-723.

Ambraseys, N. N. and Jackson J.A., 1998. Faulting associated with historical and recent earthquakes in the Eastern Mediterranean region, *Geophysical Journal International* **133**(2), 390–406.

Anderson, J. G., Wesnousky S.G. and Stirling M.W., 1996. Earthquake size as a function of fault slip rate, *Bulletin of the Seismological Society of America* **86**(3), 683–690.

ANSI/ANS-2.30, 2015. *ANSI/ANS-2.30- Criteria for Assessing Tectonic Surface Fault Rupture and Deformation at Nuclear Facilities* Published by the American Nuclear Society (2015)

Azzaro, R., Bella D., Ferreli L., Michetti A.M., Santagati F., Serva L., Vittori E., 2000. First study of fault trench stratigraphy at Mt. Etna volcano, southern Italy: understanding holocene surface faulting along the Moscarello fault, *J. Geodynamics* **29**, 187–210.

Baumont, D., Scotti, O., Courboulex F. and Melis, N., 2004. Complex kinematic rupture of the Mw 5.9, 1999 Athens earthquake as revealed by the joint inversion of regional seismological and SAR data, *Geophysical Journal International* **158**(3), 1078-1087.

Belabbes, S., Meghraoui, M., Çakir, Z. and Bouhadad, Y., 2009. InSAR analysis of a blind thrust rupture and related active folding: the 1999 Ain Temouchent earthquake (Mw 5.7, Algeria) case study, *Journal of Seismology* **13**(4), 421-432.

Bell, J.W., Amelung, F. and Henry, C.D., 2012. InSAR analysis of the 2008 Reno-Mogul earthquake swarm: evidence for westward migration of Walker lane style dextral faulting, *Geophysical Research Letters* **39**(18).

Bignami, C., Burrato, P., Cannelli, V., Chini, M., Falcucci, E., Ferretti, A., Gori, S., Kyriakopoulos, C., Melini, D., Moro, M., Novali, F., Saroli, F., Stramondo, S., Valensise G. and Vannoli, P., 2012. Coseismic deformation pattern of the Emilia 2012 seismic sequence imaged by Radarsat-1 interferometry, *Annals of Geophysics* **55**(4), 790-795.

Blaser, L., Krüger, F., Ohrnberger, M. and Scherbaum F., 2010. Scaling relations of earthquake source parameter estimates with special focus on subduction environment, *Bulletin of the Seismological Society of America* **100**(6), 2914–2926.

Blumetti, A.M., Esposito, E., Ferreli, L., Michetti, A.M., Porfido, S., Serva, L., Vittori, E., 2002. New data and reinterpretation of the November 23, 1980, M 6.9 Irpinia-Lucania earthquake (Southern Apennines) coseismic surface effects, Large scale vertical movements and related gravitational processes, *Studi Geologici Camerti*, Special Issue, 2002, 19–27.

Bonilla, M.G., Mark R.K. and Lienkaemper J.J., 1984. Statistical relations among earthquake magnitude, surface rupture length, and surface fault displacement, *Bulletin of the Seismological Society of America* **74**(6), 2379–2411.

Brcic, R., 2016. Sentinel-1 InSAR Browse Service Image of the October 2016 Central Italian Earthquakes, available at http://doi.org/10.5281/zenodo.168516 (last accessed 5 October 2018).

Brocher, T.M., Baltay, A.S., Hardebeck, J.L., Pollitz, F.F., Murray, J.R., Llenos, A. L., Schwartz D.P., Blair J.L., Ponti D.J., Lienkaemper J.J., Langenheim V.E., Dawson T.E., Hudnut K.W., Shelly D.R., Dreger D.S., Boatwright J., Aagaard B.D., Wald D.J., Allen R.M., Barnhart W.D., Knudsen K.L., Brooks B.A. and Scharer K.M., 2015. The Mw 6.0 24 August 2014 South Napa earthquake, *Seismological Research Letters*, **86**(2A), 309-326.

Bürgmann, R., Ayhan, M.E., Fielding, E.J., Wright, T.J., McClusky, S., Aktug, B., Demir, C., Lenk, O. and Türkezer, A., 2002. Deformation during the 12 November 1999 Düzce, Turkey, earthquake, from GPS and InSAR data, *Bulletin of the Seismological Society of America* **92**(1), 161-171.

Cakir, Z., Meghraoui, M., Akoglu, A.M., Jabour, N., Belabbes, S. and Ait-Brahim, L., 2006. Surface deformation associated with the Mw 6.4, 24 February 2004 Al Hoceima, Morocco, earthquake deduced from InSAR: implications for the active tectonics along North Africa, *Bulletin of the Seismological Society of America* **96**(1), 59-68.

Cheloni, D., De Novellis, V., Albano, M., Antonioli, A., Anzidei, M., Atzori, Avallone S.A., Bignami C., Bonano M., Calcaterra S., Castaldo R., Casu F., Cecere G., De Luca C., Devoti R., Di Bucci D., Esposito A., Galvani A., Gambino P., Giuliani R., Lanari R., Manunta M., Manzo M., Mattone M., Montuori A., Pepe A., Pepe S., Pezzo G., Pietrantonio G., Polcari M., Riguzzi F., Salvi S., Sepe V., Serpelloni E., Solaro G., Stramondo S., Tizzani P., Tolomei C., Trasatti E., Valerio E., Zinno I. and Doglioni C., 2017. Geodetic model of the 2016 Central Italy earthquake sequence inferred from InSAR and GPS data, *Geophysical Research Letters* **44**(13), 6778-6787.

Civico, R., Pucci, S., Villani, F., Pizzimenti, L., De Martini, P. M., Nappi, R., and Open EMERGEO Working Group, 2018. Surface ruptures following the 30 October 2016 M w 6.5 Norcia earthquake, central Italy, *Journal of Maps*, **14**(2), 151-160.

Dawson, J., Cummins, P., Tregoning, P. and Leonard, M., 2008. Shallow intraplate earthquakes in Western Australia observed by interferometric synthetic aperture radar, *Journal of Geophysical Research: Solid Earth* **113**(B11). B11408.

Dawson, J. and Tregoning, P., 2007. Uncertainty analysis of earthquake source parameters determined from InSAR: A simulation study, *Journal of Geophysical Research: Solid Earth*, **112**(B9).

Delouis, B., Giardini, D., Lundgren, P. and Salichon, J., 2002. Joint inversion of InSAR, GPS, teleseismic, and strong-motion data for the spatial and temporal distribution of earthquake slip: application to the 1999 Izmit mainshock, *Bulletin of the Seismological Society of America* **92**(1), 278, 299.

Dogan, B. and Karakaş, A., 2013. Geometry of co-seismic surface ruptures and tectonic meaning of the 23 October 2011, Mw 7.1 van earthquake (east Anatolian region, Turkey), *Journal of Structural Geology* **46**, 99-114.

Dowrick, D. and Rhoades D., 2004. Relations between earthquake magnitude and fault rupture dimensions: How regionally variable are they? *Bulletin of the Seismological Society of America* **94**(3), 776–788.

Elliott, J.R., Nissen, E.K., England, P.C., Jackson, J.A., Lamb, S., Li, Z., Oehlers, M. and Parsons, B., 2012. Slip in the 2010-2011 Canterbury earthquakes, New Zealand, *Journal of Geophysical Research: Solid Earth* **117**. B03401.

EMERGEO Working GROUP. (2019, January 21). Il terremoto etneo del 26 dicembre 2018, M w 4.9: rilievo degli effetti di fagliazione cosismica superficiale. Zenodo. http://doi.org/10.5281/zenodo.2545555

Ferrario, M. F. and Livio, F., 2018. Characterizing the Distributed Faulting During the 30 October 2016, Central Italy Earthquake: A Reference for Fault Displacement Hazard Assessment, *Tectonics* **37**(5), 1256-1273.

Fialko, Y., Sandwell, D., Simons, M. and Rosen, P., 2005. Three-dimensional deformation caused by the Bam, Iran, earthquake and the origin of shallow slip deficit, *Nature* **435**(7040), 295-299.

Foumelis M., 2016. Amatrice Earthquake - Sentinel-1 TOPS - Vertical Motion, available at http://doi.org/10.5281/zenodo.165502 (last accessed 5 October, 2018)

Funning, G.J., Parsons, B., Wright, T.J., 2007. Fault slip in the 1997 Manyi, Tibet earthquake from linear elastic modelling of InSAR displacements, *Geophysical Journal International* **169**(3), 988-1008.

Gülen, L., Pinar, A., Kalafat, D., Ozel, N., Horasan, G., Yilmazer, M. and Işikara, A.M., 2002. Surface fault breaks, aftershock distribution, and rupture process of the 17 August 1999 Izmit, Turkey, earthquake, *Bulletin of the Seismological Society of America* **92**(1), 230-244.

Gürpinar, A., Serva, L., Livio, F. and Rizzo, P.C., 2017. Earthquake-induced crustal deformation and consequences for fault displacement hazard analysis of nuclear power plants, *Nuclear Engineering and Design* **311**, 69-85.

International Atomic Energy Agency (IAEA), 2010. *Seismic Hazards in Site Evaluation for Nuclear Installations Specific Safety Guide: IAEA Safety Standards Series No. SSG-9*, Vienna, Austria.

Johnston, A.C., 1994. Seismotectonic interpretations and conclusions from the stable continental region seismicity database, in *The Earthquake of Stable Continental Regions. Volume 1: Assessment of Large Earthquake Potential*, (J. F. Schneider - Editor), Technical Report to Electric Power Research Institute TR 102261-V1, Palo Alto, California, 4-1–4-103

Kobayashi, T., Tobita, M., Nishimura, T., Suzuki, A., Noguchi, Y. and Yamanaka, M., 2011. Crustal deformation map for the 2011 off the Pacific coast of Tohoku Earthquake, detected by InSAR analysis combined with GEONET data, *Earth Planets and Space* **63**(7), 621.

Lee, W. J., Lu, Z., Jung, H. S. and Ji, L., 2017. Measurement of small co-seismic deformation field from multi-temporal SAR interferometry: application to the 19 September 2004 Huntoon Valley earthquake, *Geomatics, Natural Hazards and Risk* **8**(2), 1241-1257.

Livio, F. A., Michetti, A. M., Vittori, E., Gregory, L., Wedmore, L., Piccardi, L., Tondi E., Roberts G., Blumetti A.M., Bonadeo L., Brunamonte F., Comerci V., Di Manna P., Ferrario M.F., Faure Walker J., Frigerio C., Fumanti F., Guerrieri L., Iezzi F., Leoni G., McCaffrey K., Mildon Z., Phillips R., Rhodes E., Walters R.J., Wilkinson M., 2016. Surface faulting during the August 24, 2016, Central Italy earthquake (Mw 6.0): preliminary results, *Annals of geophysics*, **59**(5), DOI: https://doi.org/10.4401/ag-7197 .

Livio, F., Serva, L. and Gürpinar, A., 2017. Locating distributed faulting: Contributions from InSAR imaging to probabilistic fault displacement hazard analysis (PFDHA), *Quaternary International*, **451**, 223-233.

Lohman, R.B. and Simons, M., 2005. Locations of selected small earthquakes in the Zagros mountains, *Geochemistry, Geophysics, Geosystems* **6**(3).

Mai, P. M. and Beroza G.C., 2000. Source scaling properties from finite-fault-rupture models, *Bulletin of the Seismological Society of America* **90**(3), 604–615.

Mason, D.B., 1996. Earthquake magnitude potential of the intermountain seismic belt, USA, from surface-parameter scaling of late Quaternary faults, *Bulletin of the Seismological Society of America* **86**, 1487–1506.

Massonnet, D., Rossi, M., Carmona, C., Adragna, F., Peltzer, G., Feigl, K. And Rabaute, T., 1993. The displacement field of the Landers earthquake mapped by radar interferometry, *Nature* **364**(6433), 138-142.

Moss, R. E. S., Stanton, K. V. and Buelna, M. I., 2013. The impact of material stiffness on the likelihood of fault rupture propagating to the ground surface, *Seismological Research Letters*, **84**(3), 485-488.

Mercier de Lepinay, B., Deschamps, A., Klingelhoefer, F., Mazabraud, Y., Delouis, B., Clouard, V., Hello, Y., Crozon, Y., Marcaillou, B., Graindorge, D., Vall_ee, M., Perrot, J., Bouin, M.P., Saurel, J.M., Charvis, P. and St-Louis, M., 2011. The 2010 Haiti earthquake: a complex fault pattern constrained by seismologic and tectonic observations, *Geophysical Research Letters* **38**(22), L22305.

Michetti, A. M., Brunamonte, F., Serva, L., Vittori, E., 1996. Trench investigations of the 1915 Fucino earthquake fault scarps (Abruzzo, Central Italy): geological evidence of large historical events, *Journal of Geophysical Research: Solid Earth*, **101**(B3), 5921-5936.

Mohammadioun, B. and Serva, L., 2001. Stress Drop, Slip Type, Earthquake Magnitude and Seismic Hazard, *Bulletin of the Seismological Society of America*, **91**(4), 694–707

Nappi, R., Alessio, G., Gaudiosi, G., Nave, R., Marotta, E., Siniscalchi, V., Civico, R., Pizzimenti, L., Peluso, R., Belviso, P. and Porfido, S., 2018. The 21 August 2017 Md 4.0 Casamicciola earthquake: First evidence of coseismic normal surface faulting at the Ischia volcanic island, *Seismological Research Letters*, **89**(4), 1323-1334.

Okada, Y., 1985. Surface deformation due to shear and tensile faults in a half-space, *Bulletin of the seismological society of America*, **75**(4), 1135-1154.

Pallister, J. S., McCausland, W. A., Jónsson, S., Lu, Z., Zahran, H. M., El Hadidy, Aburukbah A.S., Stewart, I.C.F., Lundgren, P.R., White, R.A. and Moufti M.R.H., 2010. Broad accommodation of rift-related extension recorded by dyke intrusion in Saudi Arabia, *Nature Geoscience*, **3**(10), 705.

Parsons, B., Wright, T., Rowe, P., Andrews, J., Jackson, J., Walker, R., Khatib, M., Talebian, M., Bergman, E. and Engdahl, E.R., 2006. The 1994 Sefidabeh (eastern Iran) earthquakes revisited: new evidence from satellite radar interferometry and carbonate dating about the growth of an active fold above a blind thrust fault, *Geophysical Journal International* **164**(1), 202-217.

Pathier, E., Fielding, E.J., Wright, T.J., Walker, R., Parsons, B.E. and Hensley, S., 2006. Displacement field and slip distribution of the 2005 Kashmir earthquake from SAR imagery, *Geophysical Research Letters* **33**(20). L20310.

Peltzer, G. and Rosen, P., 1995. Surface displacement of the 17 May 1993 Eureka Valley, California, earthquake observed by SAR interferometry, *Science* **268**(5215), 1333-1336.

Pezzopane, S.K. and Dawson, T.E., 1996. *Fault displacement Hazard: a Summary of Issues and Information. Seismotectonic Framework and Characterization of Faulting at Yucca Mountain.*

Pucci, S., De Martini, P. M., Civico, R., Villani, F., Nappi, R., Ricci, T., Azzaro, R., Brunori, C.A., Caciagli, M., Cinti, F.R., Sapia, V., De Ritis, R., Mazzarini, F., Tarquini, S., Gaudiosi, G., Nave, R., Alessio, G., Smedile, A., Alfonsi, L., Cucci, L. and Pantosti D., 2017. Coseismic ruptures of the 24 August 2016, Mw 6.0 Amatrice earthquake (central Italy), *Geophysical Research Letters* **44**(5), 2138-2147.

Rymer, M.J., 1992. The 1992 Landers earthquake and surface faulting, *Earthquakes & Volcanoes* (USGS), **23**(5), 209-218.

Shirahama, Y., Yoshimi, M., Awata, Y., Maruyama, T., Azuma, T., Miyashita, Y., Mori H., Imanishi, K., Takeda, N., Ochi, T., Otsubo, M., Asahina, D. and Miyakawa A., 2016. Characteristics of the surface ruptures associated with the 2016 Kumamoto earthquake sequence, central Kyushu, Japan, *Earth, Planets and Space* **68**(1), 191.

Simons, M., Fialko, Y. and Rivera, L., 2002. Coseismic deformation from the 1999 Mw 7.1 Hector Mine, California, earthquake as inferred from InSAR and GPS observations, *Bulletin of the Seismological Society of America* **92**(4), 1390-1402.

Stein, R.S., 1999. The role of stress transfer in earthquake occurrence, *Nature* **402**(6762), 605–609.

Stirling, M.W., S. G.Wesnousky, and Shimazaki, K., 1996. Fault trace complexity, cumulative slip, and the shape of the magnitude–frequency distribution for strike-slip faults: A global survey, *Geophysical Journal Int*ernational **124**(3), 833–868.

Stirling, M.W., Rhoades, D. and Berryman, K., 2002. Comparison of earth scaling relations derived from data of the instrumental and preinstrumental era, *Bulletin of the Seismological Society of America* **92(**2), 812–830.

Stirling, M. W., M. C. Gerstenberger, N. J. Litchfield, G. H. McVerry, W. D. Smith, J. Pettinga, and Barnes P., 2008. Seismic hazard of the Canterbury region, New Zealand: New earthquake source model and methodology, *Bulletin of the New Zealand Society for Earthquake Engineering* **41**, 51–67.

Stirling, M., Goded, T., Berryman, K. and Litchfield, N., 2013. Selection of earthquake scaling relationships for seismic-hazard analysis, *Bulletin of the Seismological Society of America*, **103**(6), 2993-3011.

Stock, S., and Smith, E.G.C., 2000. Evidence for different scaling of earthquake source parameters for large earthquakes depending on fault mechanism, *Geophysical Journal International* **143(**1), 157–162.

Strasser, F. O., Arango M. C. and Bommer J.J., 2010. Scaling of the source dimensions of interface and intraslab subduction-zone earthquakes with moment magnitude, *Seismological Research Letters* **81(**6), 941–950.

Taymaz, T., Wright, T.J., Yolsal, S., Tan, O., Fielding, E., Seyitoglu, G., 2007. Source characteristics of the 6 June 2000 Ortae Çankırı (central Turkey) earthquake: a synthesis of seismological, geological and geodetic (InSAR) observations, and internal deformation of the Anatolian plate, *Geological Society, London, Special Publications* **291**(1), 259-290.

Toda, S., Stein, R.S., Lin, J. and Sevilgen, K., 2011. *Coulomb 3.3 User Guide*.

Treiman, J. A., Kendrick, K. J., Bryant, W. A., Rockwell, T. K. and McGill, S.F., 2002. Primary surface rupture associated with the M w 7.1 16 October 1999 Hector Mine earthquake, San Bernardino county, California, *Bulletin of the Seismological Society of America*, **92**(4), 1171-1191.

Vakov, A.V. (1996). Relationships between earthquake magnitude, source geometry and slip mechanism, *Tectonophysics* **261(**1–3), 97–113.

Vittori, E., Deiana, G., Esposito, E., Ferreli, L., Marchegiani, L., Mastrolorenzo, G., Michetti, A.M., Porfido, S., Serva, L., Simonelli, A.L., Tondi E., 2000. Ground effects and surface faulting in the September–October 1997 Umbria–Marche (Central Italy) seismic sequence, *Journal of Geodynamics*, **29**(3-5), 535-564.

Vittori, E., Di Manna, P., Blumetti, A. M., Comerci, V., Guerrieri, L., Esposito, E., Michetti, A.M., Porfido, S., Piccardi, L., Roberts, G.P., Berlusconi, A., Livio, F., Sileo, G., Wilkinson, M., McCaffrey, K.J.W., Phillips, R.J., Cowie, P.A., 2011. Surface faulting of the 6 April 2009 Mw 6.3 L'Aquila earthquake in central Italy, *Bulletin of the Seismological Society of America* **101**(4), 1507-1530.

Walters, R.J., Elliott, J.R., D'Agostino, N., England, P.C., Hunstad, I., Jackson, J.A., Parsons, B., Phillips, R.J. and Roberts, G., 2009. The 2009 L'Aquila earthquake (central Italy): a source mechanism and implications for seismic hazard, *Geophysical Research Letters* **36**(17). L17312.

Wells, D.L. and Coppersmith, K.J., 1993. Likelihood of surface rupture as a function of magnitude, *Seismological Research Letters* **64**(1), 54.

Wells, D.L. and Coppersmith, K.J., 1994. New empirical relationships among magnitude, rupture length, rupture width, rupture area and surface displacement, *Bulletin of the Seismological Society of America* **84**, 974–1002.

Wesnousky, S. G., 2008. Displacement and geometrical characteristics of earthquake surface ruptures: Issues and implications for seismic hazard analysis and the process of earthquake rupture, *Bulletin of the Seismological Society of America* **98(**4), 1609–1632.

Yen, Y.T. and Ma K.F., 2011. Source-scaling relationship for M 4.6–8.1 earthquakes, specifically for earthquakes in the collision zone of Taiwan, *Bulletin of the Seismological Society of America* **101(**2), 464–481.

Youngs, R. R., Arabasz, W.J., Anderson, R.E., Ramelli, A.E., Ake, J.P., Slemmons, D. B., McCalpin, J. P., Doser, D. I., Fridrich, C. J., SwanIII, F. H., Rogers, A. M., Yount, J. C., Anderson, L. W., Smith, K. D., Bruhn, R. L., Knuepfer, L. K., Smith, R. B., dePolo, C. M., O'Leary, K.W., Coppersmith, K.J., Pezzopane, S. K., Schwartz, D. P., Whitney, J. W., Olig, S. S. and Toro G.R., 2003. A methodology for probabilistic fault displacement hazard analysis (PFDHA), *Earthquake Spectra* **19**,191–219.